SAR Study of Different MIMO Antenna Designs for LTE Application in Smart Mobile Handsets

Zhao, Kun; Zhang, Shuai; Ying, Zhinong; Thomas, Bolin; He, Sailing

Published in:
I E E E Transactions on Antennas and Propagation

DOI (link to publication from Publisher):
10.1109/TAP.2013.2250239

Publication date:
2013

Document Version
Early version, also known as pre-print

SAR Study of Different MIMO Antenna Designs for LTE Application in Smart Mobile Handsets

Kun Zhao, Shuai Zhang, Zhinong Ying, *Senior Member, IEEE*, Thomas Bolin, and Sailing He, *Fellow, IEEE*

***Abstract*—This paper mainly focuses on the specific absorption rate (SAR) of the dual-element LTE MIMO antenna in mobile phones. Four designs of dual-element MIMO antenna (namely, dual semi-ground-free planar inverted-F antenna (PIFA), co-located antenna, dual OG PIFA in parallel position, and dual OG PIFA in orthogonal position) are studied under four typical LTE frequency points (0.75, 0.85, 1.9, and 2.1/2.6 GHz) when the ground plane length varies from 90 to 150 mm. The SAR, when dual elements operate simultaneously, is also studied through the SAR to PEAK location spacing ratio (SPLSR) according to the FCC standard. The simulations are carried out on both an SAM head phantom and a flat phantom by CST 2011, and measurements on the flat phantom are made with iSAR and DASY4 to verify the accuracy of our simulations.**

***Index Terms*—LTE, MIMO, mobile handset, specific absorption rate.**

I. Introduction

THE electromagnetic absorption of a human body has become an important issue, as the governments strictly limit it. Due to the extensive spread of mobile handsets, the radiation of mobile phones has rapidly been given increased attention. The radiation can be evaluated by specific absorption rate (SAR), which represents the time rate of microwave energy absorption inside the tissue, as follows:

$$\mathrm{SAR} = \frac{\sigma}{2\rho}E^2 \tag{1}$$

where ρ and σ are the density (S/m) and electrical conductivity (kg/m^3) of the tissue, respectively, E is the internal induce electrical field (V/m). The SAR value is calculated as maximum of mass-averaged SAR and is strictly limited by the governments. Nowadays, two standards of SAR are adopted: Europe uses 2 W/kg averaged over 10 g tissue (over 10 g tissue means to average the SAR values in a volume with an average mass of 10 g [1]). Meanwhile, the U.S. Federal Communication Commission (FCC) requires that the SAR should be lower than 1.6 W/kg averaged over 1 g tissues in the U.S. Due to the lower limited value and smaller averaged mass, the standard from FCC (1.6 W/kg) is more difficult to satisfy than the one from EU (2 W/kg). In this paper, all the SAR values and distributions are calculated and measured based on the FCC (1.6 W/g average 1 g) standard.

As all the mobile handsets on the market must satisfy the SAR regulations from the local government, it also becomes a challenge for the engineers to design a mobile handset antenna. So far, some studies on the traditional single antenna have been done [2]–[4]. However, due to the deployment of long-term evolution (LTE), the LTE multiple-input and multiple-output (MIMO) antenna system will be mounted in the mobile phone soon (in the first step, only a dual-elements MIMO system will be used), which will bring the new problem for evaluating and optimizing the antenna's SAR reduction. Unlike a single-antenna system, the antennas will interact with other elements in an MIMO system, and this interaction will change the SAR performance of each antenna. Furthermore, in order to satisfy the application of LTE communication, the LTE MIMO antenna system in a mobile handset has more operation modes than a traditional single antenna system. Their influence on the SAR of the antennas has to be investigated as well. So far, only a few studies on the SAR of multiantenna systems have been made [5], [6]. In the present paper, the SAR performance of the MIMO antenna in single-input single-output (SISO) mode, diversity mode, and MIMO mode are investigated.

However, with the existing equipment, it's hard to measure the total SAR when the dual elements operate simultaneously, especially when the dual elements operate at different frequencies. The value of SAR to PEAK location spacing ratio (SPLSR) is utilized to evaluate the SAR performance when dual elements work at the same time [7], which is defined as

$$\mathrm{SPLSR} = (\mathrm{SAR1} + \mathrm{SAR2})/D \tag{2}$$

where SAR1 and SAR2 are the SAR values (W/kg) for elements 1 and 2, respectively, based on the FCC standard, and D is the separation distance (cm) of the two SAR peaks, as illustrated in Fig. 1. The SPLSR is required to be less than 0.3 when the separation between the dual elements is less than 5 cm from the FCC standard. However, in our study, the SPLSR values for all the distances are presented in order to show the variation.

Based on the FCC standard, the SAR value of the mobile handset needs to be measured on two kinds of phantom: the first is a specific anthropomorphic mannequin (SAM) head phantom, which mainly shows the radiation into the tissue of the human head. The other one is the flat phantom, which is for measuring the SAR when the mobile handset is close to the user's body (therefore, this case is also called "body worn").

The aim of this paper is to provide a guideline to antenna design by showing the SAR value variations of four mainstream designs of MIMO antenna with dual elements, and also present

Manuscript received August 20, 2012; revised January 29, 2013; accepted February 24, 2013. Date of publication March 07, 2013; date of current version May 29, 2013. The partial support of the Swedish VR grant (621-2011-4620) and AOARD is gratefully acknowledged.

K. Zhao, S. Zhang, and S. He are with the School of Electrical Engineering, KTH-Royal Institute of Technology, S-100 44 Stockholm, Sweden (e-mail: sailing@kth.se).

Z. Ying and T. Bolin are with Research and Technology, Corporate Technology Office, Sony Mobile Communications AB, SE-221 88 Lund, Sweden.

Color versions of one or more of the figures in this paper are available online at http://ieeexplore.ieee.org.

Digital Object Identifier 10.1109/TAP.2013.2250239

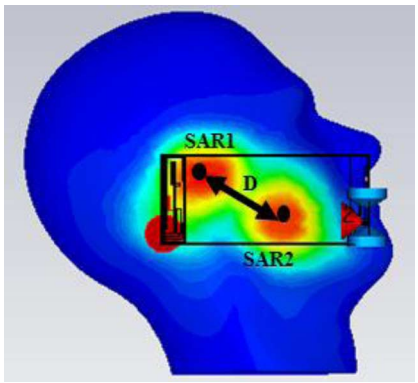

Fig. 1. The illustration of SPLSR.

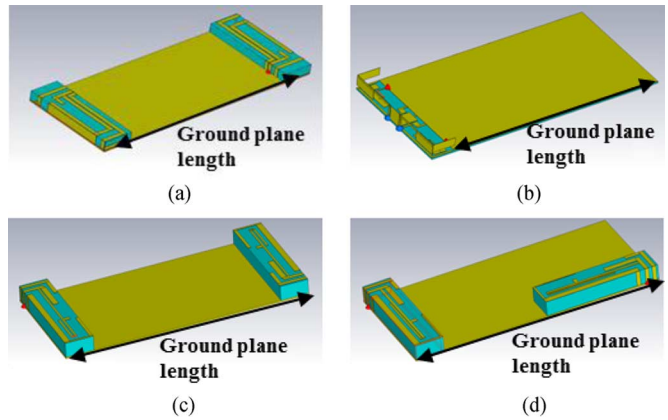

Fig. 2. The diagrams of the proposed antennas: (a) dual semi-ground-free PIFA, (b) ground-free co-located antenna, (c) dual on-ground PIFA in parallel position, and (d) dual on-ground PIFA in vertical position.

the influence from different operation modes of MIMO system on the antenna's SAR. Here, we consider four types of MIMO antennas with dual elements at four typical LTE frequencies for each design: 0.75, 0.85, 1.9, and 2.1 GHz/2.6 GHz. The results are presented by both stand-alone SAR (the SAR value when only one element is transmitting) and simultaneous SAR (the SAR value when multi antennas are transmitting simultaneously), as defined in [7]. The simulation is carried out with CST 2012, and the measurement is made with an iSAR [8] and DASY4 [9].

II. Antenna Configuration and Simulation Setup

According to 3GPP LTE Rel. 11, a dual-element MIMO antenna with dual transmitters is required in LTE mobile handset. In this paper, four designs of MIMO antenna with dual elements are presented, and their SAR performances are studied separately: dual semi-ground-free PIFAs, ground-free co-located antenna, dual on-ground (OG) PIFAs in parallel positions, and dual on-ground (OG) PIFAs in orthogonal positions. Their schematic diagrams are shown in Fig. 2. The feed positions are shown in red color: The semi-ground-free PIFA means that part of the ground plane under the PIFA antenna is removed in order to achieve a better bandwidth ("the semi-ground free" is between "ground free" and "on ground"). The size of the ground plane clearance is 13 mm on each end for semi-ground-free PIFA and is 11 mm for ground-free co-located antenna (the ground plane clearance size is 0 for OG PIFAs). The antenna heights are 5.5, 7.1, 8, and 8 mm for semi-ground-free PIFA, co-located antenna, parallel OG PIFA, and orthogonal OG PIFA, respectively. In order to simulate a real mobile handset, a plastic box is utilized to cover each MIMO antenna. These four designs can represent the three most popular types of antennas in the industry: ground-free antenna, semi-ground-free antenna, and on-ground antenna. Meanwhile, both co-located MIMO antenna and separately located (dual elements located on the two ends of the ground plane) MIMO antennas are included in our proposed designs of MIMO antennas. The original ground plane lengths for semi-ground-free PIFA, co-located antenna, parallel OG PIFA, and orthogonal OG PIFA are 90, 120, 130, and 130, respectively. (However, in order to study how different ground plane length influences the SAR value for each MIMO antenna design, we scan the ground plane length from 90 to 150 mm for each MIMO antenna design in the Section III.)

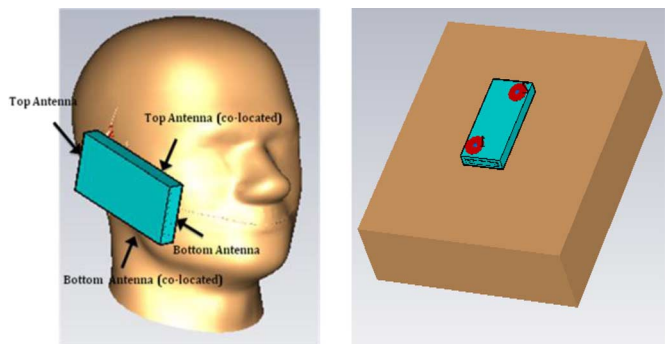

Fig. 3. The CST simulation model of (a) SAM head phantom and (b) flat phantom.

For −6 dB specification with the original ground plane length, the semi-ground-free PIFA and co-located antenna can cover 0.75 to 0.96 GHz in lower band and 1.7 to 2.7 GHz in higher band. The bandwidth of the two designs of dual OG PIFAs is between 0.75 and 0.85 GHz in lower band and 1.7 to 2.2 GHz in higher band. Considering the required band for LTE and the bandwidth of each MIMO antenna, we study four frequency points for each design: 0.75, 0.85, 1.9, and 2.6 GHz for semi-ground-free PIFA and co-located antenna; 0.75, 0.85, 1.9, and 2.1 GHz for parallel OG PIFA and orthogonal OG PIFA. The simulation setup for the SAM head phantom is shown in Fig. 3; the antenna is placed in cheek touch position in accordance with the CTIA standards [10]. The acoustic component of the cell phone is set to be 10.5 mm lower than the top of the cell phone case and the antenna ground plane is 4.5 mm away from the pinna. For co-located antennas, dual elements are both placed at the bottom of the ground plane in order to lower the SAR value. For the vertical OG PIFA, the vertical antenna is placed at the top of the ground plane. We refer to the antenna close to the ear as top antenna and the one close to the mouth as bottom antenna; for the co-located antenna, the upper element (the element upper on the back to month line) is called top antenna and lower element is bottom antenna, as also shown in Fig. 3. For the flat phantom, the antennas are placed 10 mm above the phantom [11] and face to the flat phantom.

As the antennas will be detuned when they are close to the phantoms, we set the accepted powers by the ports (the accepted power is equal to the radiated power of an antenna without ohmic losses [12], which is defined in (3)) of the MIMO antenna to constant values:

$$P_{\text{accepted}} = P_{\text{total}}(1 - |S11|^2 - |S21|^2) \tag{3}$$

where P_{total} is the total power feeds to the antenna. The accepted powers for all the study cases are set at 23 dBm, which is the maximum output power for LTE mobile handset based on the latest 3GPP standard [13]. In practice, the 23 dBm is peak value for free-space radiation power, and the corresponding SAR values in our study represent the worst-case SAR for each antenna design.

For the MIMO antenna, due to the mutual scattering effect between the multiple elements, the level of S-parameter will still influence the H-field distribution to a different extend, and this extend is mainly determined by each individual design. In our study, the S11 parameter for all our study cases (in FS, on head phantom, and on flat phantom) is smaller than -5 dB in order to keep the relative position of the main radiator the same and minimize the effect of S-parameter.

III. Simulation Results and Analysis

A. Stand-Alone SAR on SAM Head Phantom

The case when two MIMO antenna elements operate separately is studied first; one element is transmitting and the other one is receiving (terminated with a 50 ohm load). The stand-alone SAR is used to evaluate the SAR performance as the ground plane length increases from 90 to 150 mm in this case, and all the antennas are placed on the left or right cheek.

As the influence of S-parameters has been eliminated by the constant value of the accepted power, the radiation efficiency becomes an important factor determining the radiation power. The radiation efficiencies for our four proposed antennas with different ground plane lengths at 0.75 and 1.9 GHz are presented in Fig. 4 (the co-located antenna has the same efficiency on both cheeks due to its symmetric structure).

The performance at 0.85 and 2.1/2.6 GHz are similar with 0.75 and 1.9 GHz, respectively. Therefore, all the results (radiation efficiency, SAR, etc.) are only presented at 0.75 and 1.9 GHz in this section.

Bottom Antenna at 0.75 and 1.9 GHz: The SAR values of the bottom antenna with different ground plane lengths on the right or left cheek of SAM head phantom are plotted in Fig. 5 at 0.75 and 1.9 GHz.

By observing the results of radiation efficiency and SAR, we can see that they have opposite trends: the higher SAR, the larger reduction of radiation efficiency in head position, and vice versa. This can be explained by the fact that more power is absorbed by the head phantom when SAR is higher and less power is radiated out.

Generally, the values of SAR keeps decreasing when the ground plane length increases. By (1) and the previous study [14]–[17], we can know that as the ports of bottom elements are further away from the cheek of the head phantom when the ground plane is longer, it can reduce the strength of the internal induced E-field, and the SAR value is smaller as well.

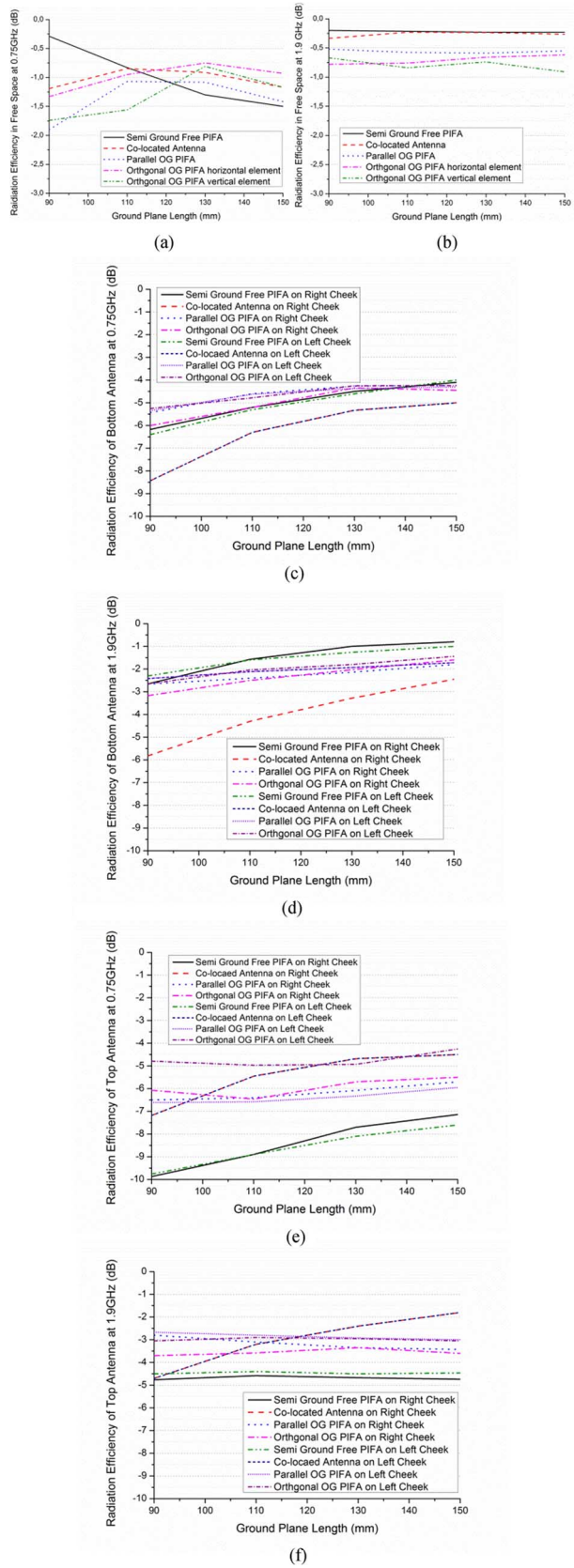

Fig. 4. The radiation efficiencies of our proposed antennas in free space at (a) 0.75 GHz and (b) 1.9 GHz, bottom antenna in head position at (c) 0.75 GHz and (d) 1.9 GHz and top antenna in head position at (e) 0.75 GHz, and (f) 1.9 GHz.

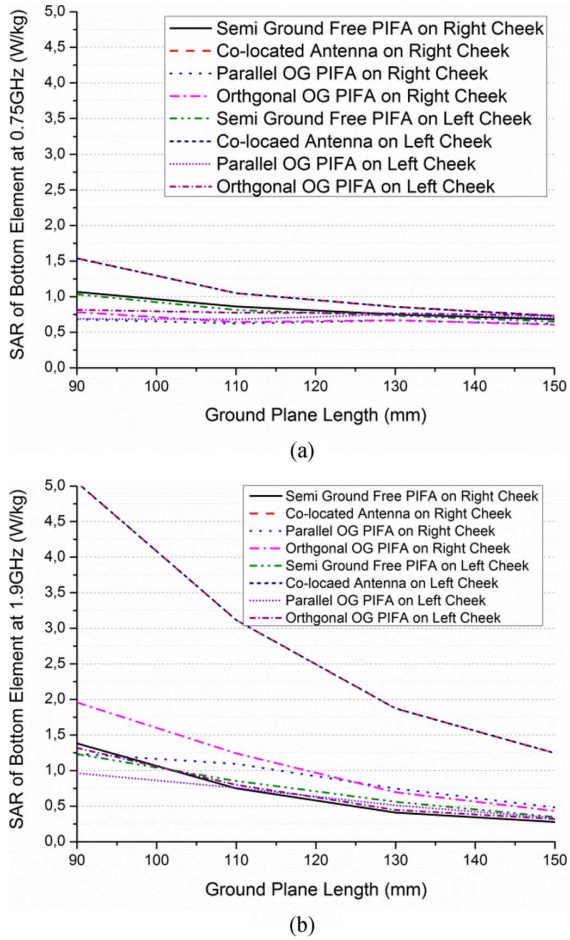

Fig. 5. The variations of stand-alone SAR value with increased ground plane length for bottom antenna at (a) 0.75 GHz and (b) 1.9 GHz.

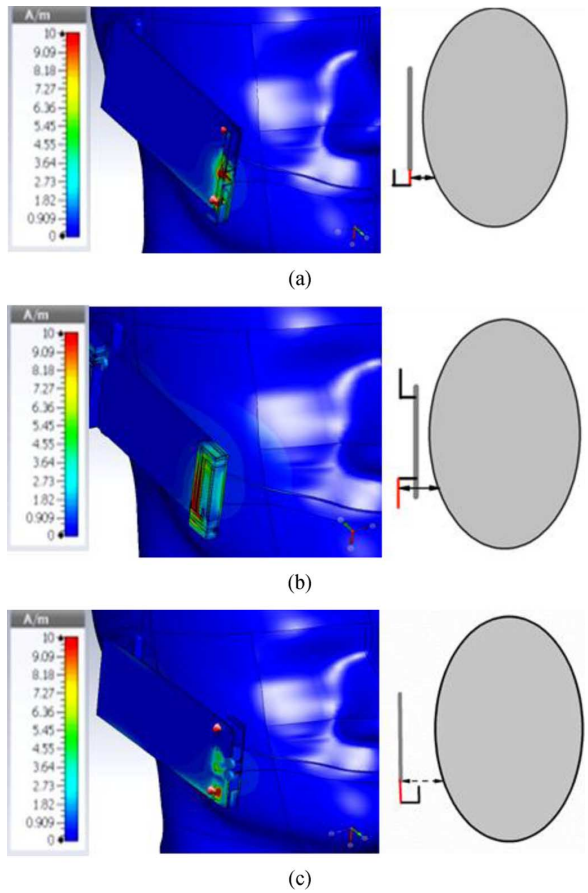

Fig. 6. The difference of radiator and H-field distribution at 1.9 GHz between (a) the co-located antennas, (b) the semi-ground-free PIFA, and (c) the inverted co-located antenna on right cheek (the radiators are shown in red).

We can also see that the SAR value of separately located antenna is different on the left and right cheeks for the bottom antenna. (The co-located antenna is symmetric on both sides, and thus the SAR value is the same on both sides.) This is mainly caused by the fact that the ports of our proposed antenna are biased to one corner of the ground plane in order to gain enough bandwidth. However, this difference is fairly small, especially when the ground plane is longer than 110 mm because the antenna and its port are quite further from the cheek on both sides. Therefore, our analysis is mainly based on the performance on the right cheek in the remaining part of the paper due to the page limit. The properties on the left cheek can be studied similarly.

The SAR on both cheeks at 1.9 GHz is shown in Fig. 5(b). We can see that it has larger SAR value than 0.75 GHz in general. The interesting phenomenon for the bottom antenna is that the co-located antenna has a much higher SAR than other designs in high band (1.9 and 2.6 GHz). The reason of this phenomenon is that the radiator of the co-located antenna in the higher band is located on the same layer as the ground plane, as seen in Fig. 6. It is much closer to the head phantom compared with other designs. Therefore, the level of SAR of the co-located antenna in higher band is quite high. If we inverted the direction of the co-located antenna, which is like in Fig. 6(c), the distance between the cheek and the radiator at 1.9 GHz of the inverted co-located antenna will be similar with the other three designs: in this case, the SAR value is reduced from 3.1 W/kg (co-located antenna in original position) to 1.7 W/kg (co-located antenna in inverted position).

Top Antenna at 0.75 GHz and 1.9 GHz: The stand-alone SARs of top antenna on head phantom are plotted in Fig. 7; the SAR value variation with increased ground plane length at 0.75 and 1.9 GHz are presented. The relation of radiation efficiency and SAR is similar with bottom antenna. The SAR difference between the left and right cheeks is even smaller for the top antenna as the pinna surface is parallel to the PCB.

For the co-located antenna, both elements are located on the bottom of the ground plane and close to the month. As the "top antenna (upper element in Fig. 3)" of co-located antenna is still on the bottom of the ground plane, it has the similar trend as the bottom one (lower element). However, we still can see that the top antenna's (upper element's) SAR of the co-located antenna is smaller than the bottom antenna (lower element), which is due to the shape of the SAM head phantom [the top antenna (upper element) is further from the surface of the head phantom than the bottom antenna]. This can be observed from Fig. 8, when the port is under the back to mouth line (position 1, i.e., bottom antenna of the co-located antenna); it is still blocked by the cheek on the side of the head phantom. However, when the port moves to the upper position (position 2, i.e., top antenna of the co-located antenna), it can be exposed to free space more due to the hollow around the eyes.

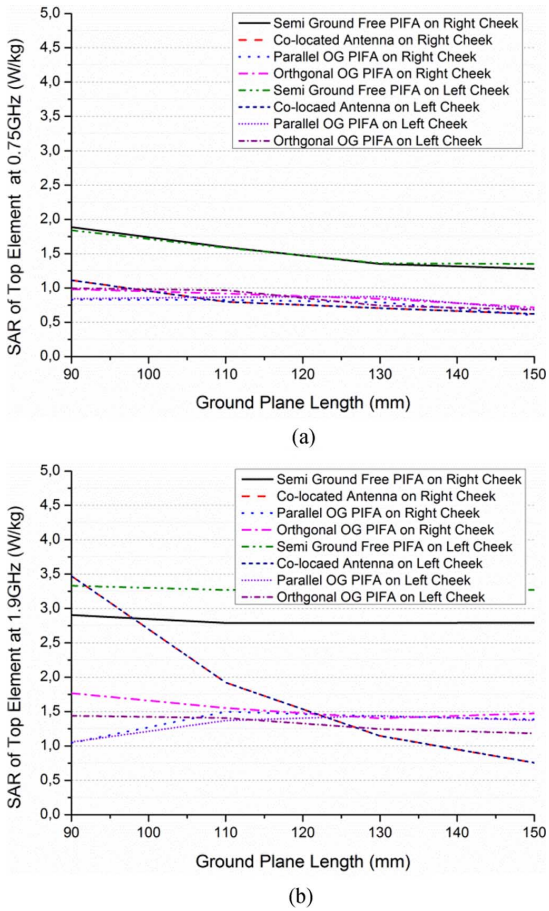

Fig. 7. The variations of stand-alone SAR value with increased ground plane length for top antenna at (a) 0.75 GHz and (b) 1.9 GHz.

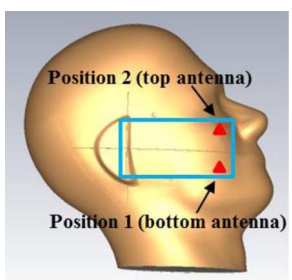

Fig. 8. The port positions for the co-located antenna.

For the other three designs of separately located MIMO antennas, we can see that the top elements have higher SAR than the bottom antenna, which agrees with our expectations, as the top elements are nearer to the head phantom than the bottom elements. Unlike the bottom elements, the variation of SAR value with the increased ground plane length of the top elements are much smaller than that of the bottom elements, which is due to the relative position of the antenna's port, and the pinna does not change with increased ground plane length. However, we can see that the SAR values at 0.75 GHz still drop as the chassis mode becomes stronger with increased ground plane length, which make the H-field distribution more uniform [2]. Furthermore, we can also see that the SAR of the semi-ground-free PIFA is larger than the two designs of OG PIFA, which illustrates the importance of the ground plane shield effect in SAR value optimization.

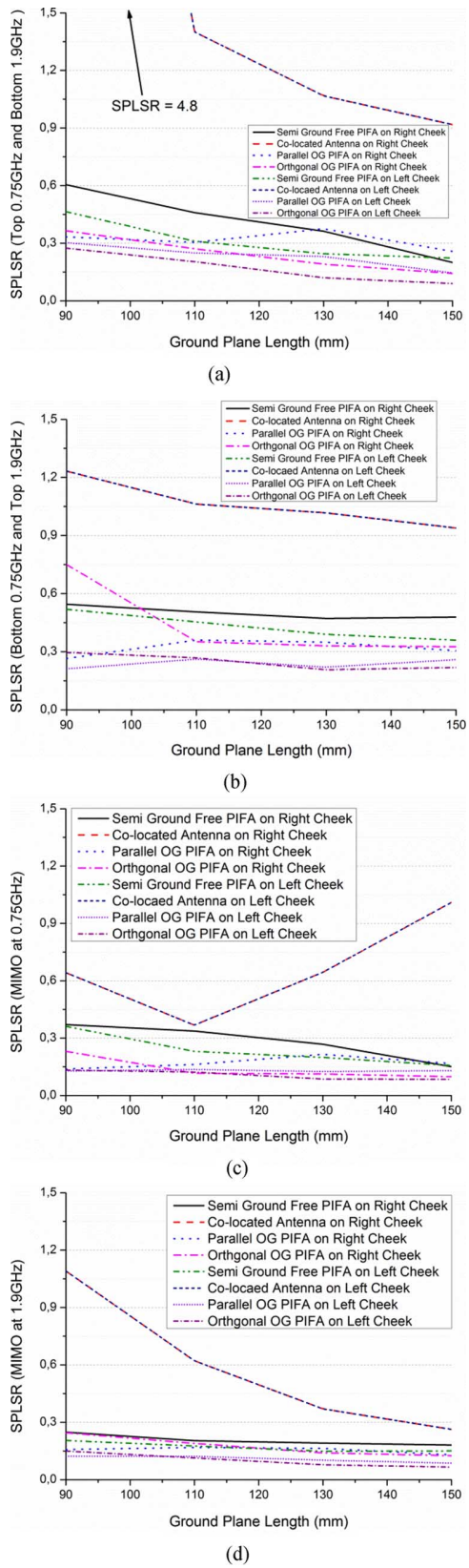

Fig. 9. The variations of SPLRS on right and left side of head phantom with increased ground plane length in (a) bottom antenna at 1.9 GHz + top antenna at 0.75 GHz, (b) bottom antenna at 0.75 GHz + top antenna at 1.9 GHz, (c) both at 0.75 GHz, and (d) both at 1.9 GHz.

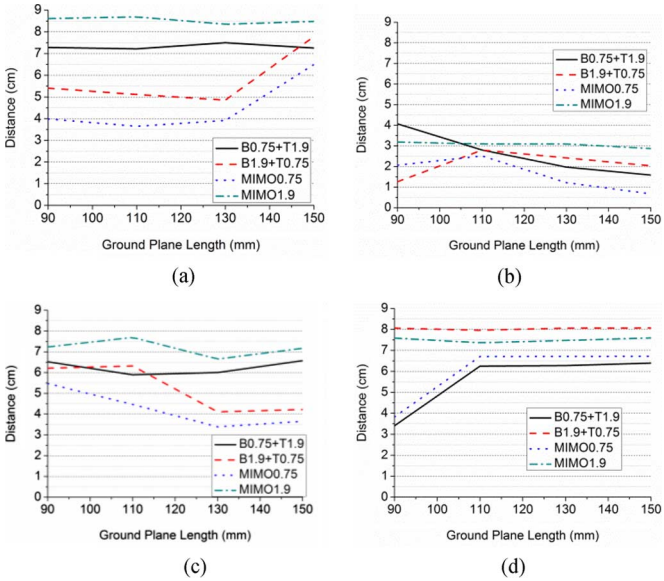

Fig. 10. The variation of the distance between two SAR hot spots on right cheek for (a) dual semi-ground-free PIFA, (b) co-located antenna, (c) parallel OG PIFA, and (d) orthogonal OG PIFA (B: bottom antenna; T: top antenna).

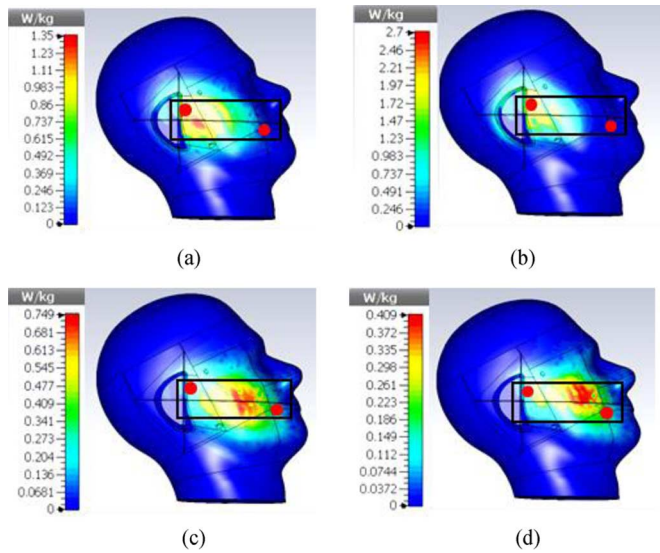

Fig. 11. The normalized SAR distribution of dual semi-ground-free PIFA on the right cheek in 110 mm ground plane length on right cheek: (a) top antenna at 0.75 GHz, (b) top antenna at 1.9 GHz, (c) bottom antenna at 0.75 GHz, and (d) bottom antenna at 1.9 GHz.

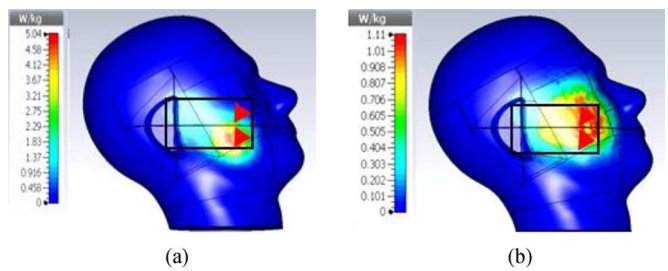

Fig. 12. The normalized SAR distribution of co-located antenna on the right cheek in 90 mm ground plane length on right cheek: (a) bottom antenna at 0.75 GHz and (b) top antenna at 1.9 GHz.

B. Simultaneous SAR on SAM Head Phantom

Different from SISO antenna, the MIMO system can have multi-elements operate simultaneously, which brings a new issue for us to study. The SAR performances when dual elements operate simultaneously are investigated next. Two cases are considered in our research. The first one is that the dual elements operate at different frequencies (one is at 0.75 GHz, and the other one at 1.9 GHz), the accepted power is set to be 23 dBm for each port. The second one is when dual elements work in the same frequency (both in 0.75 GHz and in 1.9 GHz), which can be seen as the real MIMO mode. In this case, based on the LTE standard and the definition of MIMO communication [18], we average the input power (23 dBm) to two ports. All cases are evaluated by SPLSR in (2). The variations of SPLSR on both sides of head phantom as the ground plane length increases are shown in Fig. 9.

The trend of SPLSR is more complex. Compared with the mode that dual elements operate at different frequency, the SPLSR of the MIMO mode is smaller as the input power of each port is lower and the H-field distribution is more uniformly on the whole antenna. From (2), we can see that not only the peak value of SAR but also the distance between the two hot spots of SAR plays an important role. As the value of the stand-alone SAR has been discussed in the last section, we will focus on the position variation of SAR hot spots in this part, and the analysis is mainly on the right cheek.

The variations of the distance between two SAR hot spots of the MIMO antennas on the right side of the head phantom are shown in Fig. 10.

In general, the MIMO mode at 0.75 GHz has the smallest distance, and the MIMO mode at 1.9 GHz has the largest distance. For the separately located antenna (dual semi-ground-free PIFA, parallel OG PIFA, and orthogonal OG PIFA), as the chassis mode is strong in the lower band here (0.75 GHz), the hot spots of SAR will be closer to the middle of the ground plane, which will reduce the hot-spots distance. The hot spot for the top antenna always concentrates around the pinna of the head phantom and the hot spot for the bottom element SAR is around the cheek touch point, as shown in Fig. 11 (in order to the show the positions of strongest point more clearly, all the SAR distribution in this paper is normalized by their maximum SAR).

However, when the ground plane length is extremely long or short, the chassis mode might vary dramatically, and the hot spots would move to the port or the antenna; this can change the distance between the hot spots dramatically, as one can see for the case of the 150 mm ground plane length for dual semi-ground-free PIFA or 90 mm for orthogonal OG PIFA.

For the co-located antenna, we can see that the value of SPLSR is a quite high in most cases: the closely located scheme reduces the distance between the hot spots, which makes the SPLSR become quite a challenge value for this kind of design. The distance between the hot spots is smaller when the ground plane length is larger. Two cases are quite interesting for the co-located antenna. The first one is "bottom antenna 0.75 GHz + Top antenna 1.9 GHz" with 90 mm ground plane length, as shown in Fig. 12. Although the ground plane is quite small, the distance between the two hot spots can be over 4 cm, which is much larger than the distance between the two elements.

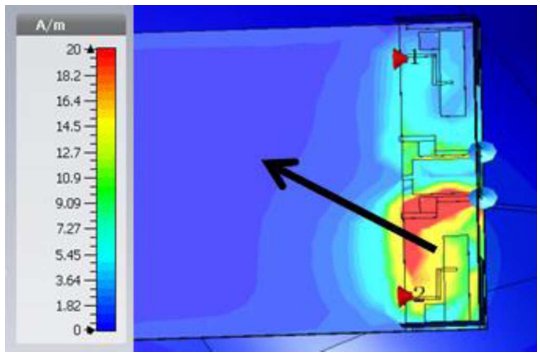

Fig. 13. The H-field of bottom antenna on the ground plane (of 90 mm length) of co-located antenna at 0.75 GHz.

Fig. 13 shows the H-field distribution of the bottom antenna (lower element) on the 90 mm ground plane at 0.75 GHz. From Fig. 13, one sees that the H-field hot spot of the bottom antenna is concentrated around the feeding and the shorting pin, which is the main source of SAR when the ground plane length is 90 mm. However, the distance between the antenna element and the user's cheek will increase as the ground plane length increases. Consequently, the H-field on the ground plane will become the main source of inducing the SAR rather than the H-field of the antenna element. From Fig. 13, we can see that the H-field distribution on the ground plane is closer to the middle line of the chassis; therefore, the corresponding SAR hot spots become closer to each other. Furthermore, the SAR hot spot of the bottom element also moves faster as it works at lower band and has a stronger chassis mode. From this case, we can see that with a longer ground plane, the distance between two SAR hot spots is not necessarily larger but can be smaller as well.

The other interesting case of co-located antenna is when both elements work at 0.75 GHz when the ground plane is fairly large (more than 110 mm). Due to the similar reason with previous case, the two hot spots are quite close, and the distance between them can be as small as 6 mm.

Based on the results from the two previous sections, we can see that the difference of the SAR on the right and left side of the head phantom is not large, especially when the ground plane length is fairly long. The chassis mode can reduce the value of stand-alone SAR effectively, but for the simultaneous SAR, a strong chassis mode will reduce the distance between the hot spots of the MIMO antenna SAR. This is an important point and needs to be traded off when designing the antenna. Furthermore, the SAR and SPLSR of the co-located antenna are quite high due to its ground-free structure and closely located scheme.

C. Study on Flat Phantom

In the industry, the flat phantom is more useful when we simulate the antenna's effect on the human body (thus, also called the "body worn" case). The case box of the antenna is placed above the flat phantom by a distance of 10 mm, which is the standard space for body SAR measurement. The same cases (stand-alone SAR and simultaneous SAR) are studied on the flat phantom as well. Basically, we can observe that the property of the SAR variation on the flat phantom is similar to that on the SAM head phantom. However, due to the simple shape of the phantom, we can still find some more interesting phenomena.

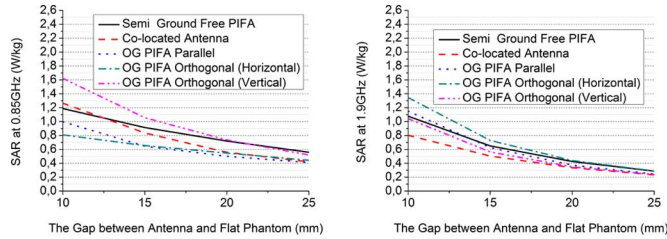

Fig. 14. The SAR value variation with increased height of antenna above the flat phantom at (a) 0.85 GHz and (b) 1.9 GHz.

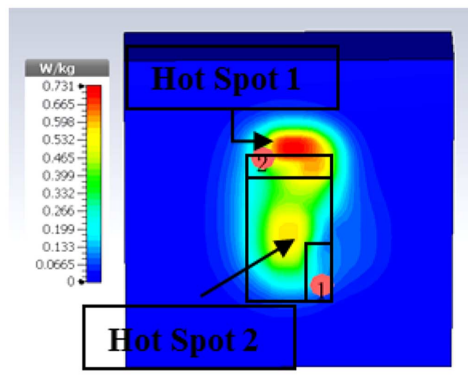

Fig. 15. The SAR distribution when only the horizontal placed OG PIFA is exciting on 10 mm above the flat phantom at 0.75 GHz.

First, the value of stand-alone SAR shows a different performance for each design. Here, instead of changing the length of the ground plane, we increase the separation gap between the antenna and the phantom from 10 to 15 mm, and then to 20 mm and finally to 25 mm (the antenna faces the flat phantom) in order to compare the SAR value more clearly.

The simulation results for the value of stand-alone SAR on the flat phantom are plotted in Fig. 14. As the flat phantom has a symmetric structure, only one element's result is presented for each MIMO antenna (the orthogonal OG PIFA has two elements' result, as it has an asymmetric structure). One interesting thing here is that the vertical element in orthogonal OG PIFA has the largest SAR; this is due to the shield effect of the ground plane, which reflects most energy to the phantom and enlarges the SAR value.

However, the level of parallel OG PIFA and the horizontal element in the orthogonal OG PIFA's SAR are quite low in the lower band, although the shield effect also exists on these two designs. The SAR and H-field distribution are shown in Fig. 15: The interesting point here is that two hot spots can be found in Fig. 15(b): one is induced by the antenna itself (hot spot 1), and the other one is induced by the coupled power on the vertical element (hot spot 2) and the chassis mode. Hot spot 1 on the top is stronger, and thus we calculate the SPLSR only for the top one. Here, due to the limitation of CST, we cannot get the exact SAR value and position of the hot spot at the middle of the ground plane, but we may get a higher SPLSR if we use this hot spot because the hot-spot distance is much smaller, and the existing algorithm may not be able to give an accurate result.

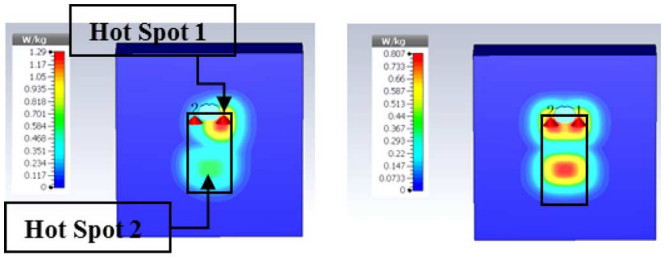

(a) (b)

Fig. 16. The normalized (a) stand-alone SAR distribution and (b) combined SAR distribution for co-located antenna in 1.9 GHz on 10 mm above the flat phantom.

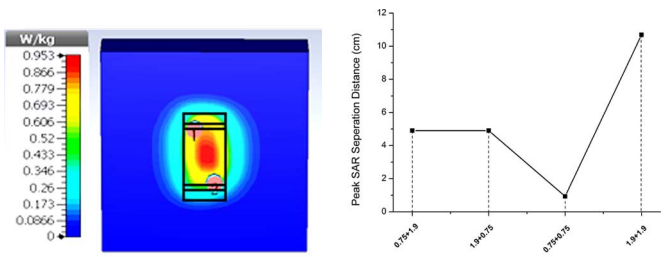

(a) (b)

Fig. 17. (a) The normalized SAR distribution of dual semi-ground-free PIFA on 10 mm above the flat phantom at 0.75 GHz; (b) the distance variation between different operating cases.

The first-order chassis mode can always influence the lower band SAR; in the meantime, the higher order chassis mode will influence the SAR in the high band. The H-field can achieve a strong density close to both ends of the ground plane [19]. For the co-located antenna, although both elements are placed on one side of the ground plane, we can still observe a small hot spot of SAR in the higher band on the other side of the ground plane [1.9 GHz; see Fig. 16(a)].

We can see the hot spot close to the bottom of the ground plane from Fig. 16(a). When the dual elements transmit simultaneously, the two hot spots become more apparent from the combined SAR distribution in Fig. 16(b).

Based on the previous studies, the strong chassis mode is helpful for reducing the level of stand-alone SAR. However, the distance between the SAR hot spots might be reduced by this strong chassis mode as well and will damage the performance of simultaneous SAR. For example, in Fig. 17, the dual semi-ground-free PIFA can achieve a quite uniform SAR distribution in 0.75 GHz, and thus, the hot-spot distance of dual elements operating at 0.75 GHz is extremely small, especially compared with the MIMO at 1.9 GHz.

IV. Measurement

In order to verify our simulation results, the stand-alone SAR for the dual semi-ground PIFA is measured on a flat phantom. The measurement is conducted on a flat phantom by iSAR and DASY4. The antenna is placed at 10, 15, 20, and 25 mm above the phantom, respectively. The Balun is connected to the antenna in order to eliminate the current on the cable, and the 50 Ω load is connected to the off element. Due to the limitations of the equipment, only the SAR at 0.85 and 1.9 GHz are measured. The photos of measurement setup of iSAR are shown in Fig. 18.

Fig. 18. The measurement setup of iSAR system.

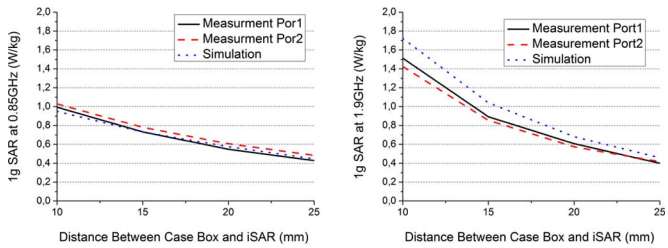

(a) (b)

Fig. 19. The measurement results on iSAR system for dual semi-ground-free PIFA at (a) 0.85 GHz and (b) 1.9 GHz.

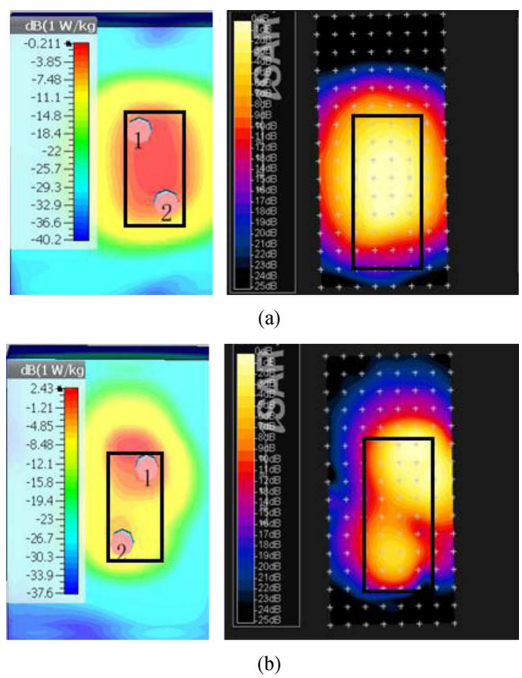

(a)

(b)

Fig. 20. The comparison between simulated and measured SAR (dB) distribution (dB) for semi-ground-free PIFA at 10 mm above the flat phantom at (a) 0.85 GHz, and (b) 1.9 GHz.

The measurement results of SAR value from iSAR are presented in Fig. 19(a) and (b). The iSAR system is a fast and easy tool to measure the SAR. We can see that simulation results agree well with the measurement results. However, due to the limited accuracy of our measurement setup, there is still a little deviation at 1.9 GHz.

The comparison between simulated and measured patterns of SAR are shown in Fig. 20; the black box on the measured picture represents the antenna's position. We can see that the results agree well with each other.

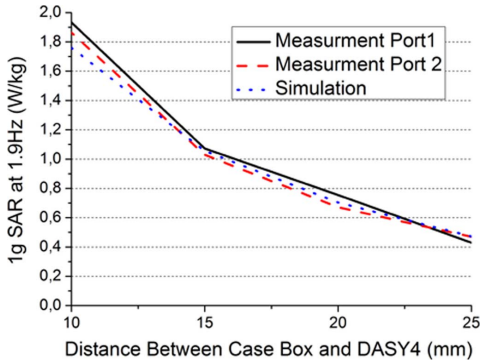

Fig. 21. The measurement results on Dasy 4 system for dual semi-ground-free PIFA at 1.9 GHz.

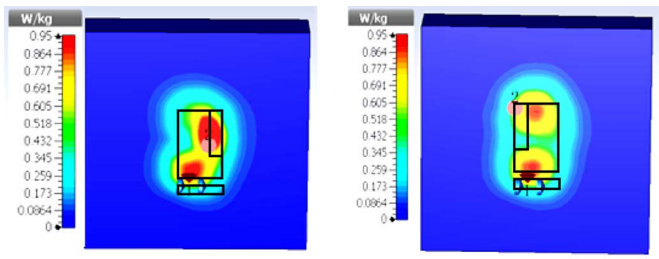

(a) (b)

Fig. 22. Simultaneous SAR at 1.9 GHz for (a) original structure and (b) improved structure.

In order to further test the accuracy of our simulation results, we use the Dasy 4 system to measure the SAR of the mock-up. However, since the DASY 4 system we used is only calibrated above 1 GHz, only the SAR at 1.9 GHz is measured.

We can see that the simulation results almost coincide with the measured results this time, which demonstrates the high accuracy of our simulation.

V. Simultaneous SAR Reduction

The value of the stand-alone SAR can be reduced by controlling the current distribution with parasitic element, slot, etc., which has been well known. For the simultaneous SAR or SPLSR, however, not only the SAR value, but also the position of the SAR hot spot is important. Therefore, we try to optimize the location of the antenna and its port to reduce the simultaneous SAR. The simulation is carried out on a flat phantom, and the proposed MIMO antenna consists of one monopole and one OG PIFA with a 104 mm ground plane, and both elements work at 1.9 GHz in MIMO mode.

The SAR distribution of the original antenna structure can be found in Fig. 22(a). It can be found that the two hot spots are quite close in this case: the distance is around 5 cm, the SPLSR is 0.3, and the simultaneous SAR can reach 1.3 W/kg, which is a dangerous value. However, in the improved structure [Fig. 22(b)], the OG PIFA is turned 180°, and the port of the OG PIFA is moved further to the monopole. We can observe that the two hot spots are separated, the distance between two hot spots are enlarged to 8.5 cm, and the value of SPLSR and the simultaneous SAR are reduced to 0.14 and 0.95 W/kg.

VI. Conclusion

The SAR performance of dual-element MIMO antennas in smart phones has been thoroughly investigated. SAM head phantoms and flat phantoms have been utilized to study these MIMO antennas' SAR properties. As MIMO systems can realize more applications than SISO antennas (MIMO mode, SISO mode, etc.), more parameters and more cases need to be investigated. In our study, we mainly focus on the influence of ground plane length on the value of stand-alone SAR and simultaneous SAR (SPLSR) on head phantom; moreover, the SAR property of different MIMO antenna designs has also been discussed.

From the results, we can see the chassis mode has a big influence on the MIMO antenna's SAR, which can change the SAR value and distribution. With a stronger chassis mode, the SAR peak value will be lower and the distribution will be more uniform; meanwhile, due to the property of the chassis mode, the efficiency of the antenna can be guaranteed. However, the hot spot of the SAR will move to the center of the ground plane, and the distance between two antenna SAR hot spots will be reduced, and the value of SPLSR will be higher. Changing the antenna position on the ground plane can optimize the SAR and SPLSR, which has been demonstrated in our paper.

From the aspect of antenna bandwidth, the semi-ground-free and ground-free structure are popularly used in order to achieve a better bandwidth. However, this kind of design will enhance the risk of SAR as the antenna can radiate directly to the head (might be also closer to the head phantom like the co-located design). The shield effect of the ground plane can reduce the value of SAR dramatically on the head phantom, as the ground plane is in the middle of the antenna and phantom. However, on the flat phantom, this effect might enlarge the SAR when the antenna faces the phantom, and the bandwidth is also a challenge for the MIMO on-ground antenna when the dimension of the antenna is limited.

Compared with the separately located antenna, the co-located antenna takes smaller volume but can keep the same bandwidth. However, the SAR is a challenge issue for it: the ground-free structure would increase the stand-alone SAR and closely located design can reduce the distance between hot spots, and deteriorating the SPLSR. The top antenna (upper element) of co-located antenna has a lower SAR level than the one at the bottom on the SAM head phantom, which is caused by uneven surface of the cheek. However, for the separately located antenna (semi-ground-free PIFA, parallel OG PIFA, and orthogonal OG PIFA), the SAR value of the top antenna is larger due to that the distance between the head phantom and the antenna is closer for the top antenna (compared with the bottom antenna).

Acknowledgment

The authors would like to thank Sony Mobile Communications AB for providing the measurement equipment for this work.

References

[1] A. Hadjem, E. Conil, A. Gati, M. F. Wong, and J. Wiart, "Analysis of power absorbed by children's head as a result of new usages of mobile phone," *IEEE Trans. Electromagn. Compat.*, vol. 52, no. 4, pp. 812–819, Nov. 2011.

[2] C. H. Chang and K. L. Wang, "Printed $\lambda/8$-PIFA for penta band WWAN operation in the mobile phone," *IEEE Trans. Antennas Propag.*, vol. 57, pp. 1381–1373, May 2009.

[3] M. Siegbahm, G. B. Babik, J. Keshvari, A. Christ, B. Derat, V. Monebhurrun, C. Penney, and M. Vogel, "An international interlaboratory comparison of mobile phone SAR caculation with CAD-based models," *IEEE Trans. Electromagn. Compat.*, vol. 48, pp. 804–811, Nov. 2010.

[4] O. Kevekäs, J. Ollikainen, T. Lehtiniemi, and P. Vainikainen, "Bandwidth, SAR, and efficeincy of internal mobile phone antennas," *IEEE Trans. Antennas Propagat.*, vol. 46, no. 1, pp. 71–84, Feb. 2004.
[5] K. Zhao, S. Zhang, Z. Ying, T. Bolin, and S. He, "SAR study of different MIMO antenna designs for LTE application in smart mobile phones," presented at the IEEE Antennas and Propag. Soc. Int. Symp. (AP-S), Chicago, IL, USA, Jul. 2012.
[6] M. Wang, L. Lin, J. Chen, D. Jackson, W. Kainz, Y. Qi, and P. Jarmuszewski, "Evaluation and optimization of the specific absorption rate for multiantenna systems," *IEEE Trans. Electromagn. Compat.*, vol. 53, no. 3, pp. 628–637, Aug. 2011.
[7] *648474 D04 Handsets Multi Xmiter and Ant v01* Federal Communications Commission, Oct. 2012.
[8] About Index SAR [Online]. Available: http://www.indexsar.com/about.html
[9] *"DASY4 V4.7 System Handbook,"* Apr. 08 ed. HAC TCoil, .
[10] "Test Plan for the Mobile Station Over the Air Performance," CTIA, Washington, DC, USA, 2010.
[11] FCC SAR Test Report, Sporton International Inc., Tao Yuan Hsien, Taiwan, R.O.C., Jan. 09, 2011.
[12] T. Wittig, "SAR," CST user group meeting 2007 [Online]. Available: Available: http://www.cst.com/Content/Documents/Events/UGM2007/05-Wittig.pdf
[13] *LTE;Evolved Universal Terrestrial Radio Access (E-UTRA); User Equipment (UE) radio transmission and reception*, 3GPP TS 36.101 , ver. 11.2.0, Release 11 [Online]. Available: http://www.3gpp.org/ftp/Specs/html-info/36101.htm (2012.09)
[14] Int. Commission on Non-Ionizing Radiation Protection, "Guidelines for Limiting Exposure to Time-Varying Electric, Magnetic, and Electromagnetic Fields (up to 300 GHz)," *Health Physical*, vol. 74, no. 4, pp. 494–522, Apr. 1998.
[15] H. Li, Y. Tan, B. K. Lau, Z. Ying, and S. He, "Characteristic mode based tradoff analysis of antenna ground plane interaction for multiple antenna terminals," *IEEE Trans. Antennas Propag.*, vol. 60, pp. 490–502, Feb. 2012.
[16] P. Vainikainen, J. Ollikainen, O. Kivekas, and I. Kelander, "Resonator-based analysis of the combination of mobile handset antenna and ground plane," *IEEE Trans. Antennas Propag.*, vol. 50, pp. 1433–1444, Oct. 2002.
[17] U. Bulus, C. T. Famdie, and K. Solbach, "Equivalent circuit modeling of ground plane radiator," presented at the Proc. German Microw. Conf. (GeMIC), Munich, Germany, Mar. 16–18, 2009.
[18] M. A. Jensen and J. W. Wallace, "A review of antenna and propagation for MIMO wireless communication," *IEEE Trans. Antennas Propag.*, vol. 52, no. 11, pp. 2810–2824, Nov. 2004.
[19] S. M. Ali and H. Gu, "Effects of ground plane current on hearing aids compatibility in the handset," *IEEE Trans. Electromagn. Compat.*, vol. 52, no. 4, pp. 837–842, Nov. 2010.

Kun Zhao was born in Zhejiang, China, in 1987. He received the B.S. degree in communication engineering from Beijing University of Posts and Telecommunications, Beijing, China, in 2010 and the M.S. degree in wireless systems from Royal Institute of Technology (KTH), Stockholm, Sweden, in 2012.

Currently, he is working toward the Ph.D. degree at the Department of Electromagnetic Engineering, KTH He has been a visiting researcher at Sony Mobile Communication AB, Sweden. His current research interests include MIMO antenna design, multiple antennas-user interactions, and body centric wireless communications.

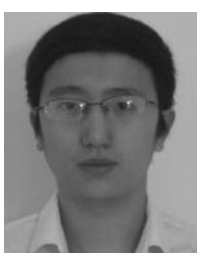

Shuai Zhang was born in Liaoning, China, in 1983. He received the B.E. degree from the University of Electronic Science and Technology of China (UESTC), Chengdu, China, in 2007 and the Ph.D. degree in electromagnetic engineering from the Royal Institute of Technology (KTH), Stockholm, Sweden, in February 2013.

Currently, he is a Research Associate at the Department of Electromagnetic Engineering, KTH. He has been a visiting researcher at the Department of Electrical and Information Technology, Lund University, Sweden, and Sony Mobile Communication AB, Sweden. His research interests include ultrawideband (UWB) antennas, MIMO antenna systems, body centric wireless communications, mm-wave antennas, RFID antennas, and multiple antennas-user interactions.

Zhinong Ying (SM'05) is currently Principal Engineer (senior expert) of antenna technology in Network Research Laboratory Research and Technology, Sony Mobile Communication AB, within Sony Group, Lund, Sweden. He joined Ericsson AB in 1995, where he became Senior Specialist in 1997 and Expert in 2003 in his engineer career at Ericsson. He has been Guest Professor in Zhejiang University, China since 2002. His main research interests are small antennas, broad and multiband antenna, multichannel antenna (MIMO) system, near-field and human body effects and measurement techniques. He has authored and coauthored over 90 papers in various of journal, conference, and industry publications. He holds more than 80 patents and pending in the antenna and mobile terminal areas. He contributed a book chapter to the well-known *Mobile Antenna Handbook* (Artech House, 3rd ed., 2008) edited by Dr. H. Fujimoto. He had invented and designed various types of multiband antennas and compact MIMO antennas for the mobile industry. One of his contributions during the 1990s is the development of nonuniform helical antenna. The innovative designs are widely used in mobile terminal industry. His patented designs have reached a commercial penetration of more than several hundreds of million products worldwide.

Dr. Ying received the Best Invention Award at Ericsson Mobile in 1996 and Key Performer Award at Sony Ericsson in 2002. He was nominated for President Award at Sony Ericsson in 2004 for his innovative contributions. He served as TPC Co-Chairmen in the International Symposium on Antenna Technology (iWAT), 2007, and served as session organizer of several international conferences, including IEEE APS, and a reviewer for several academic journals. He was a member of scientific board of ACE program (Antenna Centre of Excellent in European 6th frame) from 2004 to 2007.

Thomas Bolin the M.Sc. degree from the Applied Physics & Electrical Engineering, Linköping Institute of Technology, Sweden, in 1979

He was formerly an RF Engineer at ITT Standard Radio & Telefon AB, Stockholm, Sweden, from 1979 to 1983 in the research and development of maritime kW HF-transmitters and technical manager at Ericsson and Sony Ericson, Lund, Sweden, from 1985 to 2009 in mobile phone RF and antenna design. He is currently Master Engineer at the Network Technology Research Lab of Sony Mobile Lund with the responsibility of terminal MIMO antenna design and measurement technology. He is a member of the Sony Mobile IPR-board, and he olds some ten patents and is coauthor to a few scientific papers.

Sailing He (M'92–SM'98–F'13) received the Licentiate of Technology and the Ph.D. degree in electromagnetic theory from the Royal Institute of Technology (KTH), Stockholm, Sweden, in 1991 and 1992, respectively.

Since then, he has worked at the same division of the Royal Institute of Technology, where he has been an assistant professor, an associate professor, and a full professor. He also serves as Director for a joint research center between KTH and Zhejiang University (China). His current research interests include applied electromagnetics, electromagnetic metamaterials, optoelectronics, microwave photonics, and biomedical applications. He authored/coauthored approximately 500 papers in refereed international journals. He has given many invited/plenary talks in international conferences and has served in the leadership for many international conferences.